ARL-TR-8684 ● APR 2019

DEVCOM ARMY RESEARCH LABORATORY

An In-Depth Analysis of Competing 3-D Printed Methods for the Mobile Manufacturing of Body Armor at the Point of Need

by Tyrone L Jones, Lionel Vargas-Gonzalez, Brian Scott, Bill Goodman, and Benjamin Becker

NOTICES

Disclaimers

The findings in this report are not to be construed as an official Department of the Army position unless so designated by other authorized documents.

Citation of manufacturer's or trade names does not constitute an official endorsement or approval of the use thereof.

Destroy this report when it is no longer needed. Do not return it to the originator.

ARL-TR-8684 ● APR 2019

An In-Depth Analysis of Competing 3-D Printed Methods for the Mobile Manufacturing of Body Armor at the Point of Need

by Tyrone L Jones, Lionel Vargas-Gonzalez, and Brian Scott
Weapons and Materials Research Directorate, CCDC Army Research Laboratory

Bill Goodman
Goodman Technologies LLC, Albuquerque, NM

Benjamin Becker
HotEnd Works LLC, Oberlin, OH

REPORT DOCUMENTATION PAGE

Form Approved
OMB No. 0704-0188

1. REPORT DATE *(DD-MM-YYYY)*	2. REPORT TYPE	3. DATES COVERED (From - To)
April 2019	Technical Report	October 2017–March 2019

4. TITLE AND SUBTITLE
An In-Depth Analysis of Competing 3-D Printed Methods for the Mobile Manufacturing of Body Armor at the Point of Need

5a. CONTRACT NUMBER

5b. GRANT NUMBER

5c. PROGRAM ELEMENT NUMBER

6. AUTHOR(S)
Tyrone L Jones, Lionel Vargas-Gonzalez, Brian Scott, Bill Goodman, and Benjamin Becker

5d. PROJECT NUMBER

5e. TASK NUMBER

5f. WORK UNIT NUMBER

7. PERFORMING ORGANIZATION NAME(S) AND ADDRESS(ES)
US Army Combat Capabilities Development Command Army Research Laboratory
ATTN: FCDD-RLW-PE
Aberdeen Proving Ground, MD 21005-5069

8. PERFORMING ORGANIZATION REPORT NUMBER
ARL-TR-8684

9. SPONSORING/MONITORING AGENCY NAME(S) AND ADDRESS(ES)

10. SPONSOR/MONITOR'S ACRONYM(S)

11. SPONSOR/MONITOR'S REPORT NUMBER(S)

12. DISTRIBUTION/AVAILABILITY STATEMENT
Approved for public release; distribution is unlimited.

13. SUPPLEMENTARY NOTES

14. ABSTRACT
The goal of this work is to present results of mechanical characterization and ballistic investigation of 3-D printed alumina (Al_2O_3)-based armor plates. The 8-mm-thick plates were manufactured using two additive manufacturing-based methods: pressurized spray deposition and direct ink write (DIW). The DIW Al_2O_3 plates exhibited superior hardness, flexural strength, and density compared to the tape cast plates. Plates (90 mm × 90 mm × 8 mm) of this composition were manufactured for ballistic analysis in accordance with established ballistic characterization procedures, using a 50.8-mm-thick aluminum 6061 plate as backing and witness plates in the case of penetration or deformation. Six Al_2O_3 plates were examined ballistically (one shot per plate) against the 12.7-mm APM2 projectile (45.9 g) at an impact velocity of 840 m/s. The plates that were manufactured using the DIW method provided a higher impact resistance than the tape cast method.

15. SUBJECT TERMS
additive manufacturing, point of need, ceramic, pressurized spray deposition, direct ink write, alumina, Al_2O_3

16. SECURITY CLASSIFICATION OF:			17. LIMITATION OF ABSTRACT	18. NUMBER OF PAGES	19a. NAME OF RESPONSIBLE PERSON
a. REPORT	b. ABSTRACT	c. THIS PAGE			Tyrone Jones
Unclassified	Unclassified	Unclassified	UU	33	19b. TELEPHONE NUMBER (Include area code) (410) 278-6223

Contents

List of Figures

List of Tables

1. Introduction

The US Army Combat Capabilities Development Command's (CCDC) Army Research Laboratory has been developing the tools to create, evaluate, and provide 3-D printed ceramics for the dismounted Soldier at their point of need. Availability is arguably the most critical factor in Soldier protection, followed by weight. The overall objective to create boron carbide used for ballistic impact protection presents limitations of long lead times, fabrication of complex geometries, and expensive components. Ceramic 3-D printing offers engineering-grade ceramic components in approximately 90% less time than traditional ceramics manufacturing. Typical turnaround can be in days instead of weeks, depending on the complexity of the part. This not only allows for faster time to market but also allows for more iterations during the design process, resulting in a better end product. Additionally, 3-D printed parts can have a higher degree of complexity for weight reduction, while saving on the cost of the part because less material is required.

There are many competing methods to create 3-D printed components. This study characterized the tape cast and direct ink write (DIW) methods based on prior data established and reported in open literature. HotEnd Works (HEW) was selected to manufacture 3-D printed ceramic using the pressurized spray deposition (PSD) method, while a Goodman Technologies (GT) team was selected to manufacture 3-D printed ceramic via the DIW method.

While typical US body armor tends to use higher-performance ceramics (such as boron carbide), this study characterized 8-mm-thick alumina as the initial, cost-effective material for evaluation of the failure mechanisms and characteristics. Additionally, 6- and 8-mm-thick alumina specimens were used to develop a deeper understanding of the stages of ceramic failure caused by a small steel rod at a low-speed impact. Rod-shaped specimens, nominally 3 mm in diameter and 50 mm long, were obtained for each alumina to quantify static and quasistatic material properties. The following study compares the penetration resistance versus the manufacturing methods.

2. Processing Methodologies

2.1 Traditional Manufacturing

Traditional manufacturing of advanced ceramics typically employs various methods, the most common being die pressing or isopressing (IP) of a ceramic powder that has been combined with binding and plasticizing components.[1] To form the powder into the desired shape, tooling must be created that replicates the geometry of the components (Fig. 1). If the geometry of the component is beyond a basic shape such as a rectangle, square, or cylinder, secondary green machining using a Computer Numerical Control mill or lathe is required. Traditional manufacturing of a simple rectangle involves die pressing or IP of a prepared ceramic powder using rectangular tooling (die). The die is unloaded, and the part is then sintered at its respective densification temperature (e.g., for alumina this would be approximately 1,600 °C). If there are stringent requirements in terms of flatness, parallelism, or perpendicularity of surfaces, the component needs to be ground using diamond tooling after the sintering process.[1]

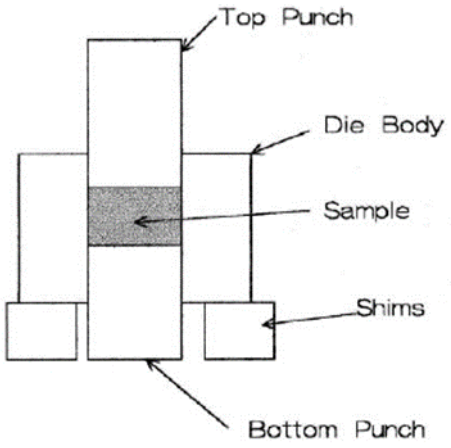

Fig. 1 Typical die press assembly

2.2 Pressurized Spray Deposition

Additive manufacturing of advanced ceramics differs mostly in terms of the initial green part formation when compared with a traditional manufacturing process. The process used by HEW is PSD. The PSD process (Fig. 2) involves the use of a proprietary blend of advanced ceramic raw material (ceramic powder) with a unique polymeric binder (support material). The polymeric support material serves as a temporary support structure during part formation to accommodate overhangs and other intricate features.[2] Powder and support materials are fed from external hoppers into the dispensing chambers and are then deposited by a high-precision

deposition nozzle. The deposition nozzle uses mechanical shaping methods that allow for a range of patterns from 0.127 to 3.81 mm (0.005 to 0.150 inch) in diameter. After the first layer is complete, formation of the next layer initiates.

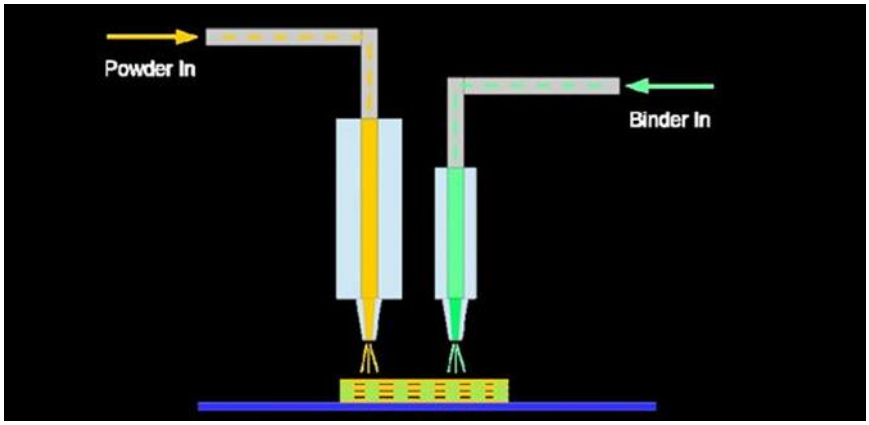

Fig. 2 PSD technology

After the formation of the component, a thermal debinding process takes place. Thermal debinding of the component is done within a wicking embedment, with an average cycle time of 24 h. The thermal debinding temperature does not exceed 150 °C. Due to the type of embedment material used, the part does not require cleaning when it is removed from the thermal debinding oven. After debinding, the component is then processed using a traditional electric or gas furnace to complete the densification. Because shrinkage occurs with the additive ceramic process, postprocessing such as diamond grinding may be required for components with tight tolerance requirements in terms of flatness, and so on. However, tooling fabrication as well as the green machining stage can be omitted due to the geometric complexity that is possible with the PSD process.

2.3 Direct Ink Writing Method

Robocasting technology is the freeform fabrication via ceramic slurries process developed at Sandia National Laboratories in the 1990s by Dr Joseph Cesarano III and Prof Paul Calvert.[3] Since then, the technology was transferred to the University of Illinois. It is now being used by several research groups and hobbyists throughout the world. Several groups have changed the name of the technology for their own reasons and robocasting is sometimes confused with direct-write assembly, DIW, micro-robotic deposition, solvent-based extrusion, extrusion freeforming, or robotic deposition. Regardless of the name, Goodman Technologies uses the process of 3-D printing via particulate pastes (a.k.a., robocasting).

In the robocasting process, software is used to partition a stereolithography format file into layers of similar thickness to the extrusion nozzle diameter. A continuous filament of particulate paste is extruded in the shape required to fill the first layer, roughly a rectangular block. Next, either the stage is moved down or the nozzle is moved up and the next layer is deposited in the required pattern. This is repeated until the 3-D part is complete. Numerically controlled mechanisms are typically used to move the nozzle in a calculated tool-path generated by a computer-aided manufacturing software package. Stepper motors or servo motors are usually employed to move the nozzle with precision as fine as nanometers.

2.4 Deliverables

The CCDC Army Research Laboratory received the following ceramic components from HEW and GT:

- Four 90-mm × 90-mm × 8-mm-thick green (not sintered) 3-D printed plates for microstructure characterization.
- Six Ø = 38.1-mm × 6.35-mm-thick plates for material property characterization.
- Fourteen 90-mm × 90-mm × 8-mm-thick plates for empirical analysis of the penetration resistance.

The data from the CoorsTek CAP 3 were generated in a prior program with the same deliverables and material characterization and ballistic characterization methodologies.

3. Material Characterization Methodologies

The DIW and PSD alumina samples were characterized through mechanical and analytical means to provide a baseline comparison of material properties as compared to that of a commercially available, traditionally processed alumina armor material, CoorsTek CAP 3 (AD-995). This sample will be referred to as IP for the remainder of the document.

The density of the as-received parts was determined by the Archimedes method. Three measurements were taken for dry, suspended, and saturated weights, respectively. Samples were boiled in water for 1 h and cooled before measuring suspended and saturated weight.

Microstructural characterization was performed on both fractured and polished specimens. The samples were scanned using a desktop scanning electron

microscope (SEM). Elemental analysis was performed using energy-dispersive X-ray spectroscopy (EDAX), which was built into the desktop SEM.

Four-point flexural strength testing was performed on all of the samples. Rectangular beams nominally 3 × 4 × 50 mm were machined by a third-party machining company from the samples as directed using the guidelines out of the ASTM C1161 standard reference document.[4] As orientation of the printed volumes was of potential concern for influence on bulk mechanical properties, two sets of beams were machined from both the DIW and PSD printed specimens. For the first variant, the 3-mm direction was machined parallel to the build direction of the parts, while the second variant had the 3-mm direction machined perpendicular to the build direction (hence the 4-mm direction facing the parallel build direction). For reference, these orientations are illustrated in Fig. 3. Six beams were tested for each of the AM alumina samples and each orientation, while 10 samples were tested for the CAP 3. Crosshead displacement was kept at 0.5 mm/min and the breaking force was measured, by which the strength was calculated.

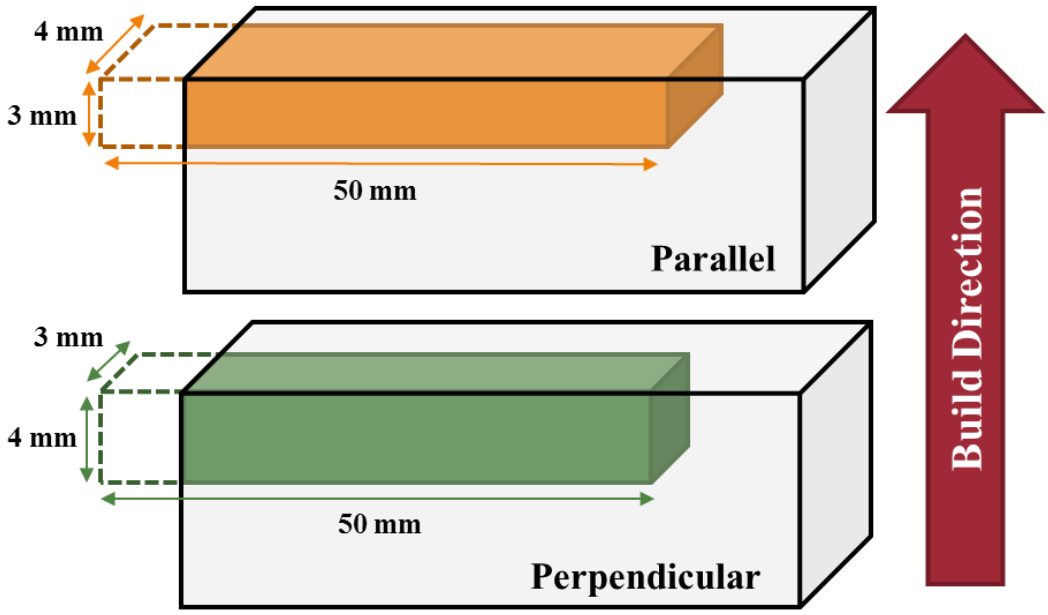

Fig. 3 Alignment of flexural strength bar samples for the DIW and PSD specimens

Hardness values for the ceramics were characterized according to the ASTM C1326 standard.[5] Ten indentations were recorded for each sample using the Knoop indentation geometry and an applied 19.6 N (2 kgf) load for 15 s. Any unacceptable indentations were thrown out and re-indented until 10 acceptable indentations were recorded. The width of the indentations was used to calculate the relative hardness value.

4. Ballistic Characterization Methodology

Depth of penetration (DOP) or residual penetration experiments, shown in Fig. 4, were designed to determine the relative ballistic performance of different ceramic materials. For DOP testing, a projectile is fired into a ceramic tile attached to a semi-infinite thick metal plate such that the projectile penetrates through the ceramic tile and then into the metal plate without deforming the back surface. These experiments avoid the fundamental problem of V_{50} ballistic dependence on armor design (e.g., front-to-back plate ratio and material), require fewer shots than V_{50} tests, and have a sensitivity equivalent to that of other ballistic test methods.[6] The change in penetration into the metal plates provides a comparison by which to rank the performance of the ceramic materials. The target configuration used for these experiments is illustrated in Figs. 4 and 5. The target consisted of a 90 × 90 mm ceramic tile at a nominal thickness of 8 mm, backed by two aluminum alloy 6061 (AA6061, MIL-DTL-32262) plates of 50.8-mm (2-inch) thickness.[7] An epoxy resin, Dureflex Optical Aliphatic Polyether Polyurethane Grade A4700, was used to attach each tile to the front surface of the first 50.8-mm (2-inch) plate. AA6061 was chosen as a well-characterized and readily available residual penetration material. The aluminum plates were also expected to provide better resolution than steel backer plates. No cover plate was employed.

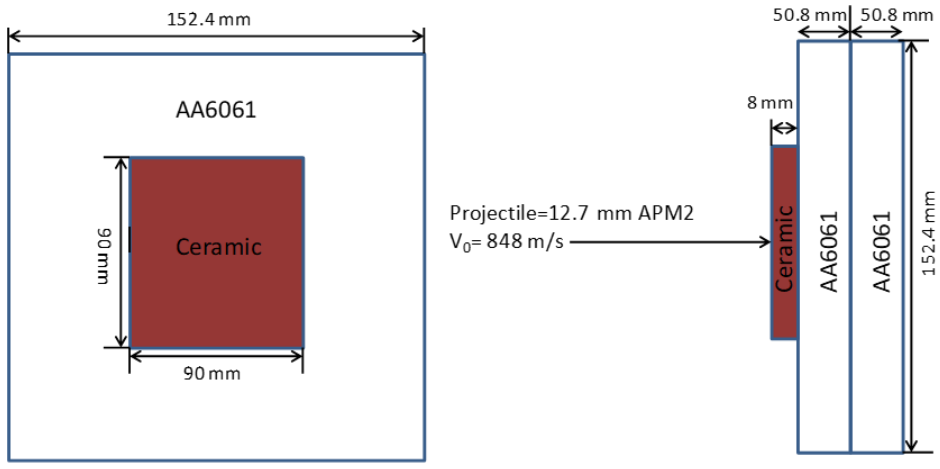

Fig. 4 Sketch of ceramic composite sample

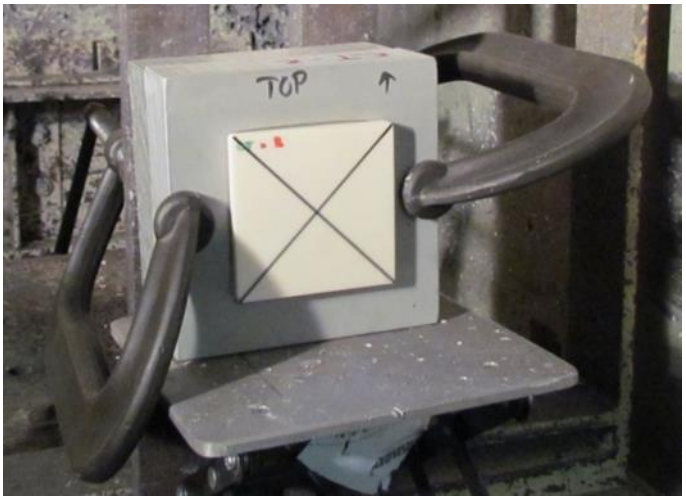

Fig. 5 Initial conditions of ceramic composite samples in fixture

All ballistic impact experiments were conducted at the CCDC Army Research Laboratory. Three experiments were performed for each alumina manufacturing process. The IP ceramic tiles were the reference material. The test projectile was the copper-jacketed 12.7-mm APM2, which includes a hardened steel core penetrator with a length of 47.6 mm (1.875 inches), a diameter of 10.87 mm (0.428 inch), and an aspect ratio of 4 (Fig. 6). The nominal projectile weight was 46 g, and core density was 7.85 g/cm^3.

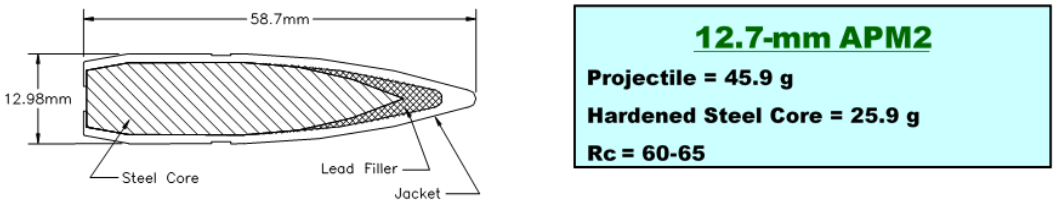

Fig. 6 Cross section of a 12.7-mm APM2

The impact velocity used for all experiments was nominally 848 m/s (2,782 ft/s), although some shots varied from 824 m/s (2,704 ft/s) up to 872 m/s (2,861 ft/s). This variability could be due to interior barrel conditions, differences in the APM2 material properties, or gun operator influence such as projectile powder measurements. The impact velocity was intentionally chosen to produce a range of measurable residual penetrations, while being consistent with real-world ballistic impact conditions. Measurement of the projectile pitch, projectile yaw, and velocity was accomplished using a Hewlett-Packard 150-kV Flash X-ray Imaging System in two orthogonal planes. All residual penetration measurements were obtained by sectioning the AA6061 plates to reveal a cross section. Electrical discharge machining was used to section all penetration cavities, and measurements were

made using vernier calipers to the deepest portion at the cavity, as indicated in Fig. 7. Measurement of the "a" value avoids errors that could be caused by deformation of the aluminum block around the cavity entrance.[6]

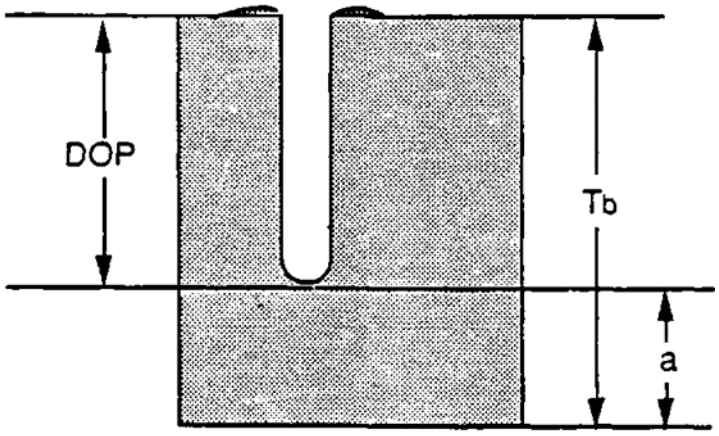

Fig. 7 Measurement of residual penetration

5. Results and Discussion

5.1 Material Characterization

The DIW, PSD, and IP alumina samples were characterized for theoretical density using the Archimedes method. The calculated density was compared with a theoretical density for alumina of 3.97 g/cm^3. While it was not known if the samples included any sintering aids, it was assumed that the density would be generally consistent to the standard value for alumina. The calculated values are listed in Table 1. The IP alumina sample exhibited a theoretical density characteristic of solid-state sintered ceramic specimens. The DIW sample exhibited a high theoretical density of 97.28%, indicative of good sintering and low porosity from defects. The PSD sample yielded the lowest theoretical density. The lack of closed surface porosity was apparent during the Archimedes immersion. It is worth noting that the surfaces of the PSD samples exhibited a high degree of rust a few days after the immersion. Subsequent analysis indicated that the surfaces were coated with iron, presumably from the grinding tool used to plane the as-received surfaces. Iron shavings embedded into the open surface of the PSD sample, leading to the observable rust.

Table 1 Density values for all alumina specimens

Specimen	Calculated density (g/cm^3)	Theoretical density (%)	Standard deviation theoretical density (%)
IP	3.82	96.29	0.31
PSD	3.43	86.64	0.89
DIW	3.86	97.28	0.10

The three samples were ground and polished to a mirror finish (< 1 μm) and imaged using the desktop SEM. The three microstructures, taken at 1000×, are shown in Fig. 8. The IP grain structure is equiaxed, and no visible inclusions or secondary phase defects are evident. Porosity is generally localized to the grain boundaries, with intragranular porosity in the larger grains (from high grain boundary mobility during sintering). The DIW microstructure is very similar to that of the IP sample; however, the sample is much more refined in grain size, indicating that the starting particle size distribution was finer than the IP. Porosity in the DIW is evident at the grain boundaries, with fewer large pores on average. The PSD microstructure is very different to that of IP and DIW. The morphology of the microstructure is that of the agglomerated alumina powder and binder particles used in the spray deposition process. The structure indicates that the binder particles did not pack effectively well, leading to the high porosity evident, and the result of the low measured sintered densities. Within the agglomerates, the structure is generally fine and well sintered.

There were defects within the DIW and PSD samples, which were inferred to be indicative of each utilized printing process. Images of these characteristic defects are shown in Fig. 9. For DIW, there were large pores (150–250 μm) on the polished surface. These were later attributed to trapped air pores from the direct write process. The defects in PSD were attributed to porosity and leftover residual carbon derived from the binder additives used in both the agglomerates and the jetting process.

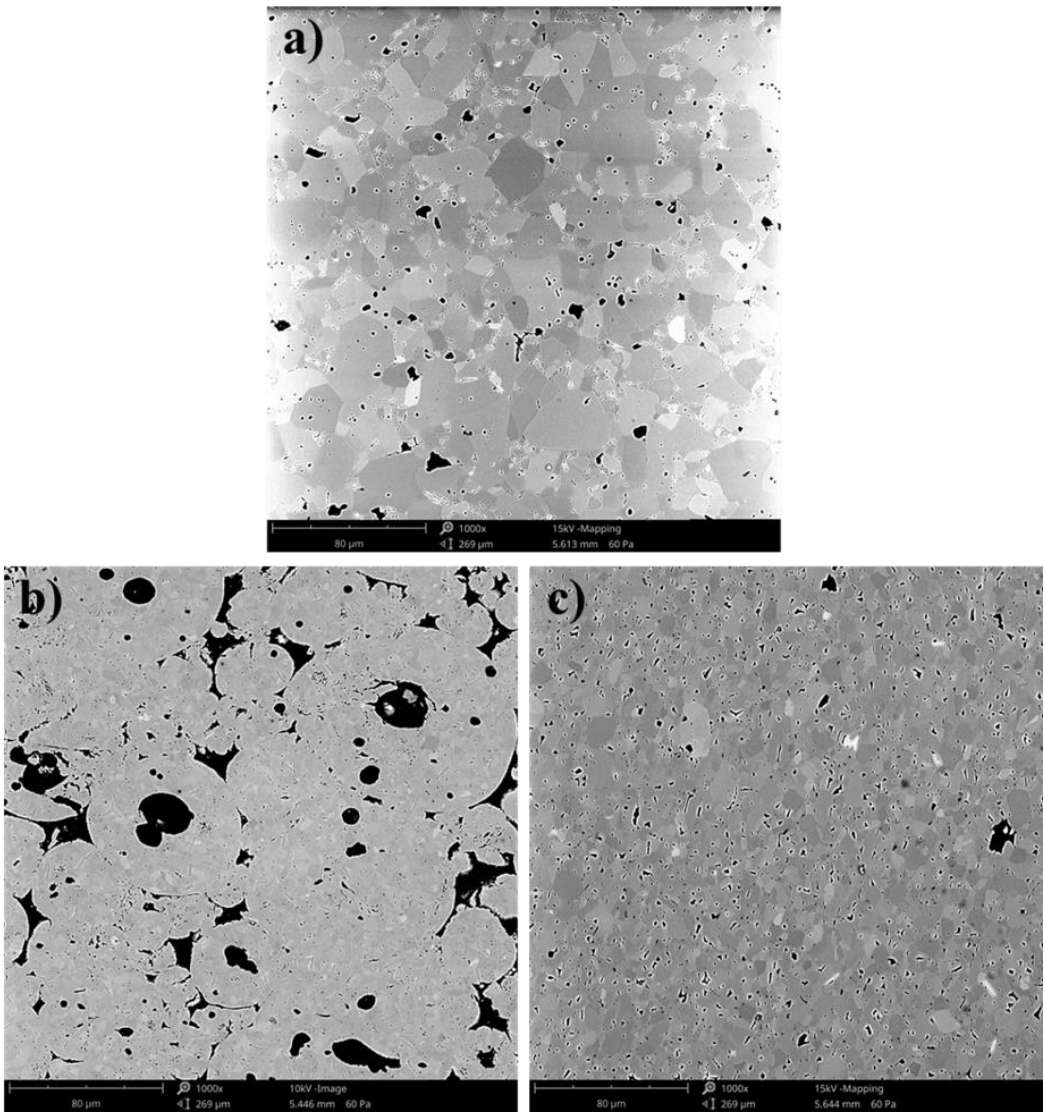

Fig. 8 SEM micrographs (1000×) for a) IP, b) PSD, and c) DIW

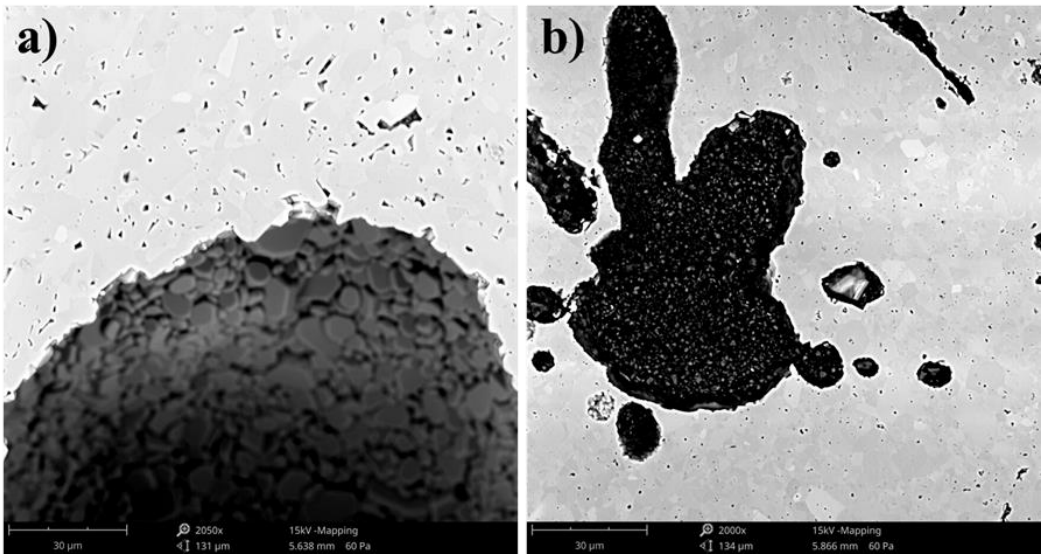

Fig. 9 SEM micrographs (2000×) for a) DIW and b) PSD showing characteristic defects in each sample from AM processing

The DIW and PSD specimens were analyzed for elemental composition using the EDAX detector in the desktop SEM, and the images for the representative areas with their respective element maps are shown in Fig. 10. The DIW sample consists of only aluminum and oxygen, with no signs of impurities or binder char. The dark areas of the PSD material, however, are full of carbon left over from the binder thermolysis. On the whole, the total carbon weight percentage of the sample was measured to be 18.1 wt. % (within the entire field of view of the micrograph, not of the inset box in the image).

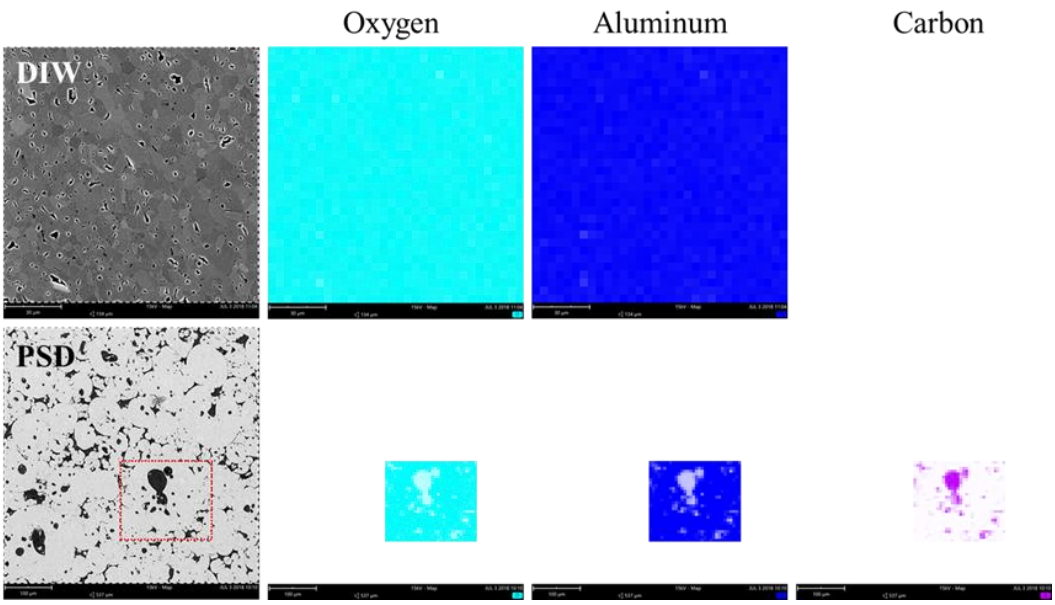

Fig. 10 EDAX elemental maps for both the DIW (top row) and PSD (bottom row). Note the area scanned for PSD is delineated in the microstructural image with the red box inset.

SEM micrographs of the fracture surfaces for the DIW and PSD samples are shown in Fig. 11. These fracture surfaces confirm the observations of the micrographs, revealing the agglomerated particle structure of the PSD and the highly sintered structure of DIW. The nature of AM printing is much harder to discern in the DIW sample as there are no indicative lines or features in the grain structure or morphology, other than the similar large pores evident from the micrographs.

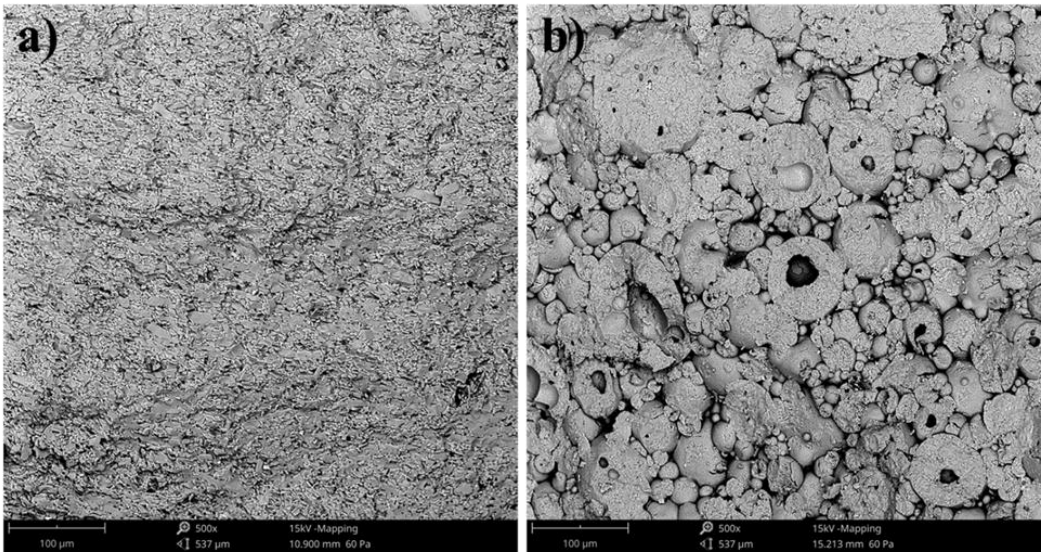

Fig. 11 SEM micrographs (500×) of the fracture surfaces for a) DIW and b) PSD specimens

Hardness values for each sample were collected at 19.6 N with a Knoop indentation geometry to calculate the relative hardness values. The hardness values are listed in Table 2 and graphed in Fig. 12 as a function of percent theoretical density. The DIW sample exhibited higher hardness values than the commercial IP material—14.80 GPa versus 13.19 GPa, respectively. As both microstructures look similar, the difference can be attributed to either the 0.99% TD increase in density, the refined grain size distribution, or both. The PSD sample exhibited the worst average hardness value of 9.83 GPa and was highly variable from one indent to the next, likely due to the highly irregular distribution of agglomerated particles, large voids within the agglomerates, and large carbon inclusions present throughout the microstructure.

Table 2 Hardness values for all alumina specimens

Specimen	Average hardness, GPa (Knoop, 2 kgf)	Standard deviation hardness, GPa (Knoop, 2 kgf)
IP	13.19	0.50
PSD	9.83	1.86
DIW	14.80	0.57

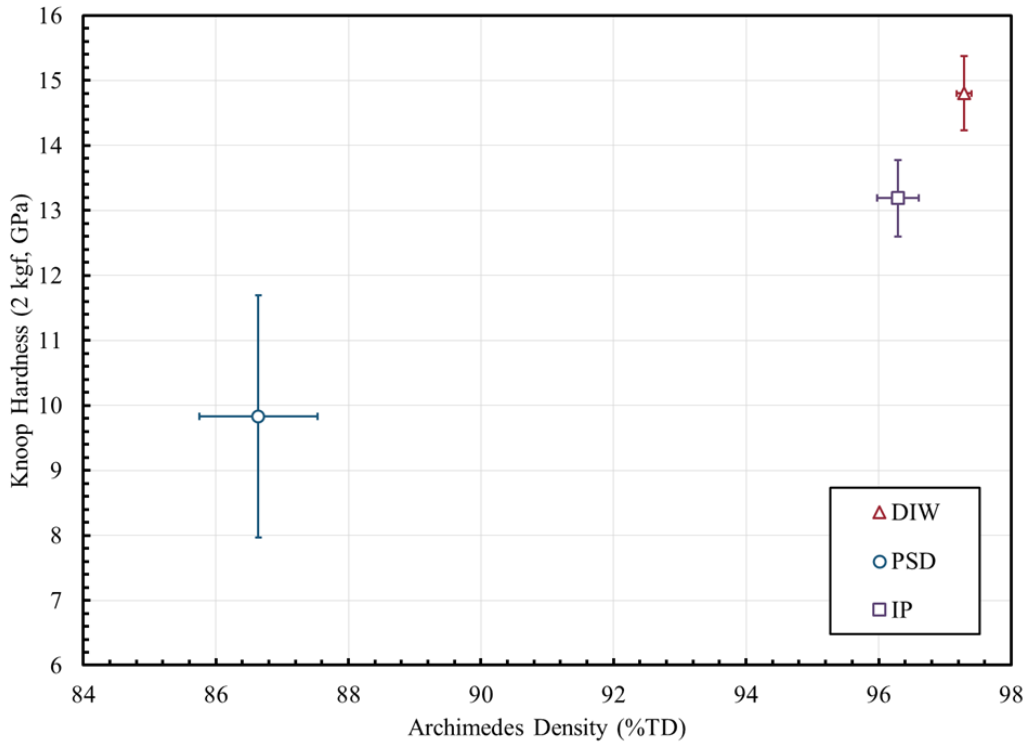

Fig. 12 The 2 kgf Knoop hardness for all three alumina samples, graphed as a function of percent theoretical density

Flexural strength values were obtained from all the IP, DIW, and PSD test bars. For the DIW and PSD specimens, both of the orientations (as described in the experimental section) were recorded. The flexural strength values are illustrated graphically in Fig. 13 and tabulated in Table 3. On average, the DIW samples outperformed the PSD samples; however, IP performed the best with the lowest amount of spread between individual values. In both cases for DIW and PSD, the knock down in strength was significant between the 3-mm cross section switch from parallel to perpendicular; therefore, there is a clear effect due to the interfaces between layers in the AM parts. When the layers are aligned perpendicular to the loading direction, the interfaces between layers are the limiting flaw and break at a lower load.

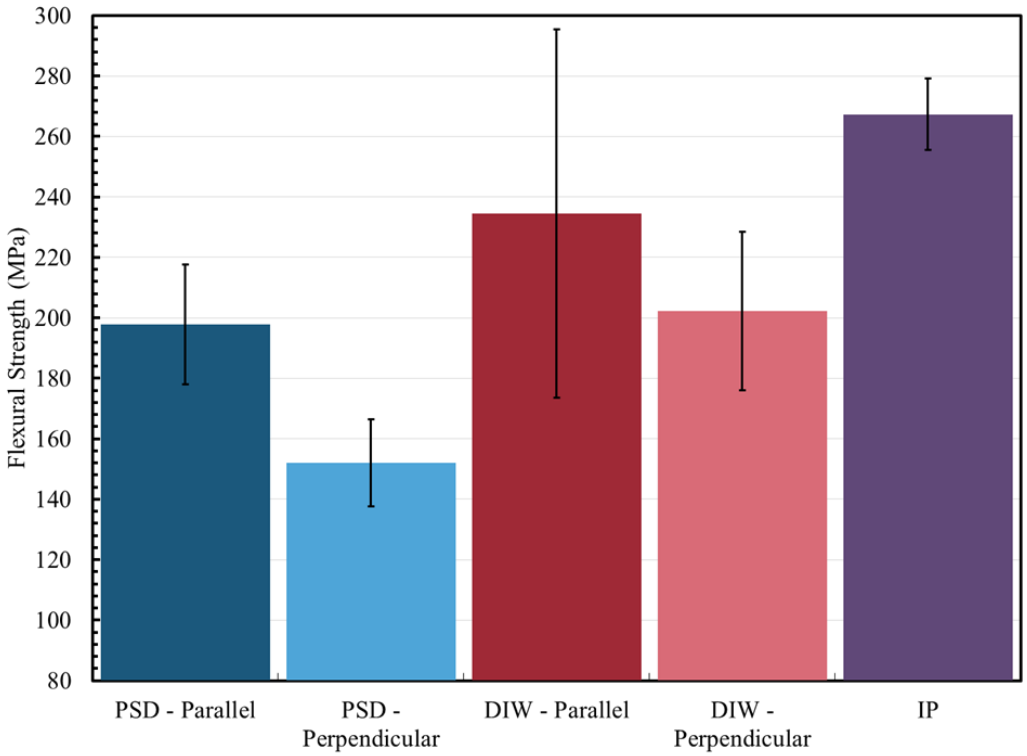

Fig. 13 Flexural strength of all alumina specimens derived through four-point testing

Table 3 Flexural strength values for all alumina specimens

Specimen	Average flexural strength (MPa)	Standard deviation flexural strength (MPa)
PSD - Parallel	198	20
PSD - Perpendicular	152	14
DIW - Parallel	234	61
DIW - Perpendicular	202	26
IP	267	12

5.2 Ballistic Characterization

5.2.1 Reference Measurements

A few shots were fired into monolithic AA6061 plates over the velocity range from 824 to 872 m/s (2,704 to 2,861 ft/s) to quantify the DOP without the ceramic, as shown in Fig. 14.[8] The primary penetrator defeat mechanism of AA6061 over the velocity regime was deceleration. Residual penetration values were then measured and plotted as a function of striking velocity to produce a baseline curve (Fig. 15). A linear regression of the reference data yielded the following equation:

$$DOP = 0.1959 \times V_{x\text{-}ray} - 84.406. \quad (1)$$

The square of the correlation coefficient, R^2, is 0.946, indicating that this curve is a reasonable approximation. For example, an experimental impact velocity of 848 m/s would be expected to result in a DOP of 81.73 mm. For these experiments, this is the DOP baseline for AA6061.

$V_{x\text{-}ray}$ (m/s)	Plate 1 (Projectile Entry Point into Plate #1)	Plate 2 (Projectile Entry Point into Plate #2)
848		
824		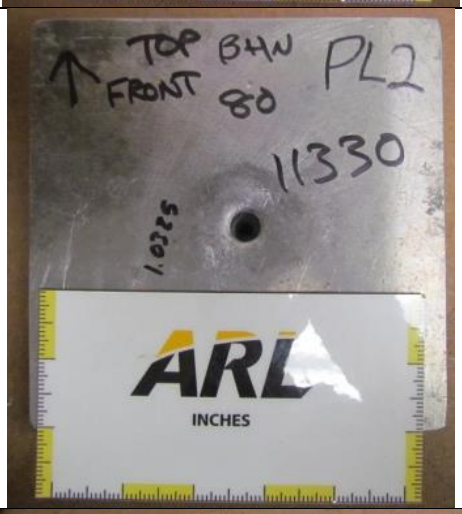
872		

Fig. 14 Ballistic penetration into AA6061

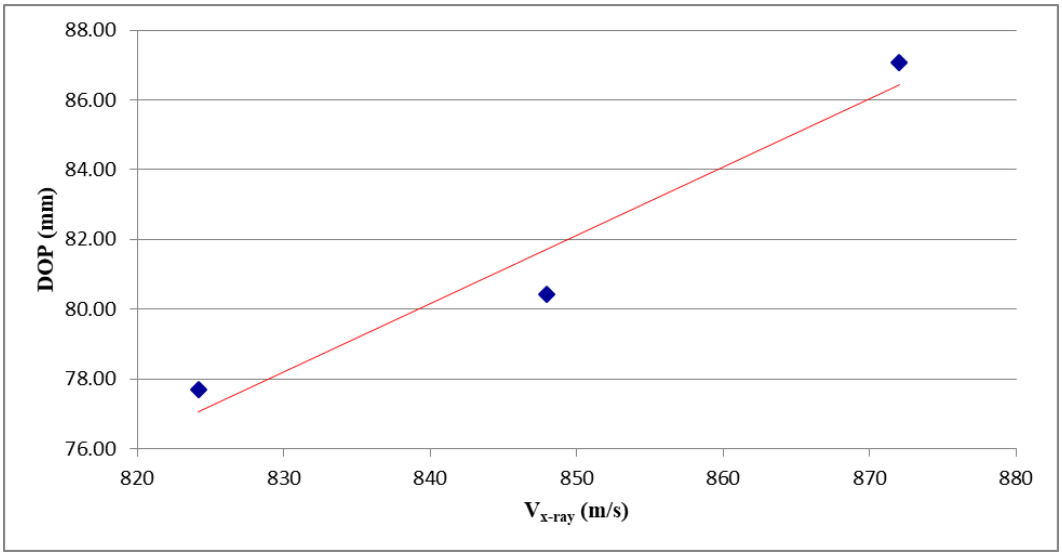

Fig. 15 Penetration of 12.7-mm APM2 into 50.4-mm AA6061 plates

Ceramic target assemblies, as previously described in Processing Methodologies, were fabricated for all materials. In general, three tiles of equal thickness (or areal density) were evaluated for each material. To adjust for variations in the actual strike velocity, all residual penetration values were normalized to a striking velocity of 848 m/s based on the empirical fit shown in Eq. 1. The correction was made as follows:

$$\text{Corrected DOP} = \text{Measured DOP} + [0.1959 \times (848 - V_{x\text{-}ray})]. \quad (2)$$

This technique has been found to be valid provided that a significant amount of the penetrator reaches the backup plate, the correction is relatively small, and the penetrator defeat mechanism has not significantly changed with velocity. In support of this assumption, observations of the size and shape of the impact showed no significant differences in penetrator cavity for the impact velocity variations. The data were obtained for the alumina tiles at a nominal thickness of 8 mm.

5.2.2 Ceramic Penetration Mechanisms

The impact measurements on the alumina tiles manufactured using the IP method are shown in Table 4. The DOP increased as the impact angle of the projectile increased. The average DOP with the correction for the IP tiles was 14.43 mm, with a standard deviation of 3.01 mm.

Table 4 Ballistic impact measurements of alumina tiles made by IP method

Shot No.	Ceramic alumina type	Striking velocity (m/s)	Total yaw (°)	DOP (mm)	DOP_{corr} (mm)
13157	IP	840	0.78	16.00	17.56
13158	IP	843	0.72	13.21	14.18
13159	IP	846	0.54	11.18	11.56

The general state of the IP tiles is shown in Fig. 16. The first photo is the front view of the residual ceramic after impact. The second photo is the cross-sectional view of the residual DOP after impact.

Fig. 16 IP alumina tiles after impact

At the ceramic tile–projectile interface, the projectile was subjected to dwell pressures that rapidly exceeded the compression strength of the core of the projectile. This resulted in shattering the projectile within microseconds. Shortly after this stage, the amplitude of the reflective (tensile) wave from the ceramic aluminum interface decomposed the IP tile, and caused it to fracture, resulting in wider penetration canal entrance, a reduction in the kinetic energy, and multiple maxima depths in the cross section of the aluminum plate.

Next, measurements on the 3-D printed alumina tiles that were manufactured using the PSD method are shown in Table 5. As with the IP tiles, the DOP into the PSD tiles increased as the impact angle of the projectile increased. The average DOP with the correction for the PSD tiles was 28.14 mm, with a standard deviation of 6.42 mm. The DOP increased as the impact angle of the projectile increased.

Table 5 Ballistic impact measurements of alumina made by PSD

Shot No.	Ceramic alumina type	Striking velocity (m/s)	Total yaw (°)	DOP (mm)	DOP_{corr} (mm)
14935	PSD	854	0.28	25.63	24.49
14942	PSD	860	0.51	33.91	31.46
14943	PSD	859	0.37	35.79	33.70
14944	PSD	868	0.57	39.93	36.05
14945	PSD	862	0.26	23.22	20.47
14946	PSD	855	0.30	24.13	22.70

The general state of the PSD tiles is shown in Fig. 17. The first photo is the front view of the residual ceramic after impact. The second photo is the cross-sectional view of the residual DOP after impact.

Fig. 17 PSD alumina tiles after impact

At the ceramic tile–projectile interface, the projectile was subjected to dwell pressures that did not exceed the compression strength of the core of the projectile. Consequently, while the projectile deformed, it did shatter. Shortly after this stage, the amplitude of the reflective (tensile) wave from the ceramic aluminum interface decomposed the PSD tile, and caused it to fracture. The projectile eroded during the deceleration, leaving a single penetration canal in the cross section of the aluminum plate.

Lastly, impact measurements on the 3-D printed ceramics that were manufactured using the DIW method are shown in Table 6. As with the IP and PSD tiles, the DOP into DIW increased as the impact angle of the projectile increased. The average DOP with the correction of the DIW alumina was 26.17 mm, with a standard deviation of 3.15 mm.

Table 6 Ballistic impact measurements of alumina tiles made by DIW method

Shot No.	Ceramic alumina type	Striking velocity (m/s)	Total yaw (°)	DOP (mm)	DOP_{corr} (mm)
14936	DIW	851	0.72	28.70	28.16
14937	DIW	852	0.57	25.73	24.89
14938	DIW	865	0.35	25.96	22.56
14939	DIW	851	0.46	28.19	27.54
14940	DIW	862	0.66	31.45	30.67
14941	DIW	863	0.43	26.16	23.18

The general state of the PSD tiles is shown in Fig. 18. The first photo is the front view of the residual ceramic after impact. The second photo is the cross-sectional view of the residual DOP after impact.

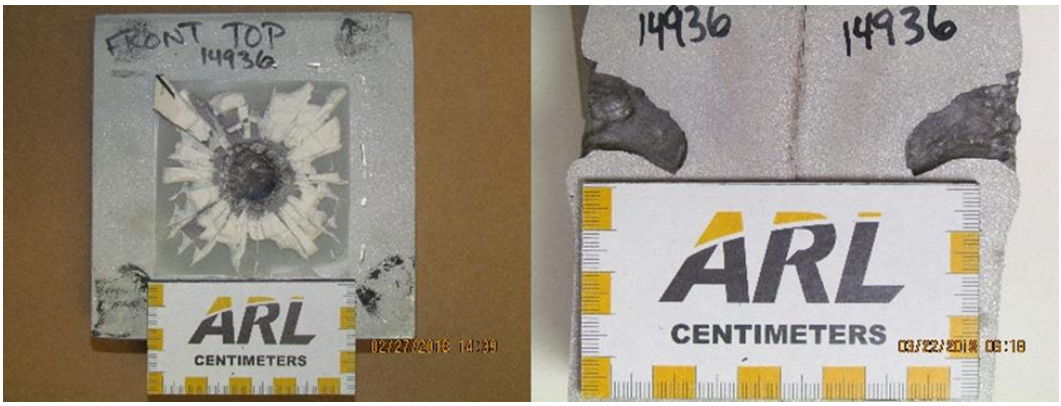

Fig. 18 DIW alumina tiles after impact

At the ceramic tile–projectile interface, the projectile was subjected to dwell pressures that did not exceed the compression strength of the core of the projectile. The projectile showed extreme deformation, but did shatter. Shortly after this stage, the amplitude of the reflective (tensile) wave from the ceramic aluminum interface decomposed the DIW tile, and caused it to fracture. The extremely deformed projectile eroded during the deceleration, leaving a wider penetration canal in the cross section of the aluminum plate than the PSD tiles.

5.2.3 Ceramic Penetration Performance

The coefficient of performance (C_p) of the ceramics compared to the reference material was calculated using Eq. 3:

$$C_p = \left(\rho_{AA6061}\right)\frac{DOP_{Base\_AA6061} - DOP_{Corr\_AA6061}}{AD_{Ceramic}}, \quad (3)$$

where DOP_{Base_AA6061} is the average expected residual depth of penetration into bare aluminum at 848 m/s; DOP_{Corr_AA6061} is the residual DOP into AA6061 after perforating the ceramic tile, corrected for the variations in striking velocity; and $AD_{ceramic}$ is the areal density of the ceramic. The DOP_{Base_AA6061} = 81.73 mm. The AD_{IP} = 31.36 kg/m^2, the AD_{PSD} = 29.54 kg/m^2, and the AD_{DIW} = 30.22 kg/m^2. The ρ_{AA6061} = 2.70 g/cm^3. The calculated C_p value provides a relative comparison of the ceramic to AA6061 (i.e., a C_p of 5 means the ceramic is 5× more weight effective than AA6061). The C_p of each alumina ceramic was calculated as shown in Table 7.

Table 7 Comparative performance of ceramics

Experiment No.	Coefficient of performance (C_p)		
	IP	**PSD**	**DIW**
1	5.52	5.39	4.77
2	5.82	4.52	5.10
3	6.04	4.43	5.29
4	…	4.15	4.81
5	…	5.49	4.58
6	…	5.20	5.22

A ceramic performance map is illustrated in Fig. 19. The alumina tiles manufactured using the IP method had superior performance over the PSD method and the DIW method. The alumina tiles manufactured from the PSD yielded the highest and lowest C_p.

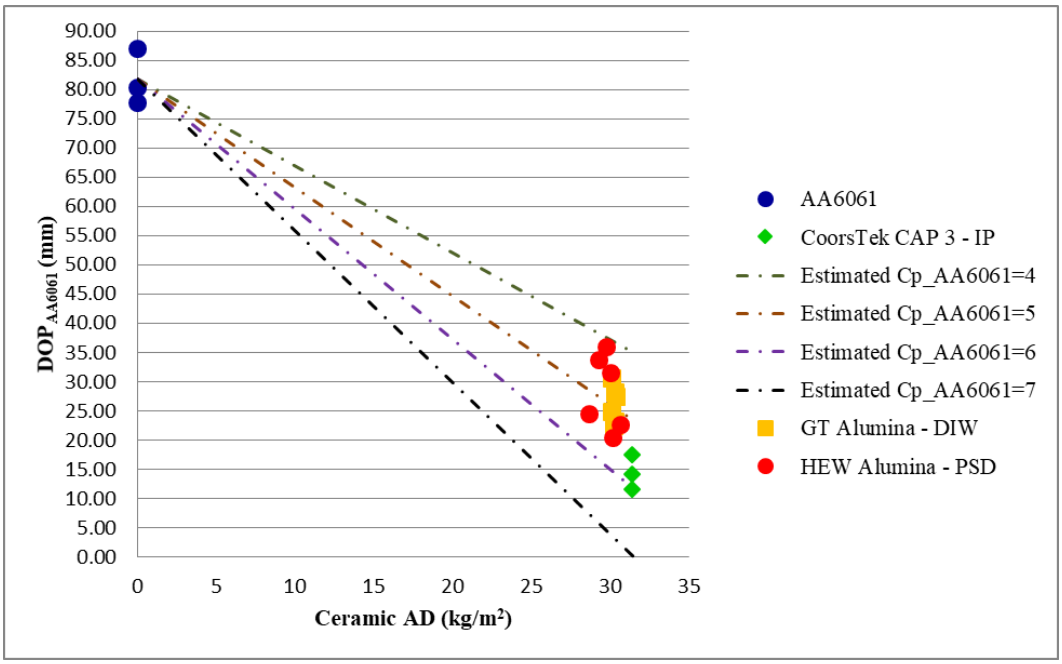

Fig. 19 Performance map for the alumina resistance of 3-D printed alumina

The average DOP, μ, and average standard deviation, σ, of the DOP are shown in Table 8. The alumina tiles manufactured by the PSD method exhibited 49% more penetration than the alumina tiles manufactured using the IP method into the aluminum witness plate. The alumina tiles manufactured using the DIW method exhibited 45% more penetration than the IP method. The IP method and DIW method had similar standard deviations, while the PSD method exhibited a 2× standard deviation to the IP method and the DIW method.

Table 8 Statistics of ballistic penetration

Specimen	μ (mm)	σ (mm)	$\Delta_{AD\text{-}995}$(mm)
IP	14.43	3.01	…
PSD	28.14	6.42	13.71
DIW	26.17	3.15	11.74

6. Conclusions

The goal of this research effort was to perform mechanical and ballistic investigations of 3-D printed alumina-based armor plates. DIW and PSD techniques were used to make alumina armor targets to test against a commercially available IP armor formulation.

Between the AM samples, DIW exhibited the highest hardness (14.80 GPa) and percent theoretical density (97.28% TD), even eclipsing the values for IP (13.19 GPa and 96.29% TD, respectively). The microstructures of the DIW samples were similar to that of the IP, but the grain sizes were lower, which could be a contributor to the hardness. The microstructure of PSD was indicative of the process, with consolidated agglomerates dominating the structure. These agglomerates contributed to the low density and hardness exhibited in PSD.

IP exhibited the highest flexural strength value at 267 MPa. DIW samples exhibited several strength values in line with IP, but there was high variability in the samples and the average value was lower at 234 MPa. The variability is likely due to the printing defects, such as the large pores between the printing lines. Both DIW and PSD samples exhibited orientation-specific strength behavior, with significant drop down in strength when the loading is perpendicular to the build direction of both the DIW and PSD specimens, indicating that the interlayer bonding between the layers is weaker than the bulk material within each printed layer. Future focus needs to be geared toward developing processing techniques and controls to limit the extent of defects from layer-by-layer approaches.

From these limited ballistic experiments, the DOP cavity profiles into the AA6061 plates were distinctly different when analyzing the IP tiles versus the PSD tile or DIW tiles. The IP tiles were 45% more efficient in arresting the penetrator than the DIW alumina tiles, and the DIW tiles were 7% more efficient in arresting the penetrator than the PSD tiles. The flexural strength of the IP tiles was high enough to achieve dwell, shatter, and subsequent erosion of the projectile core during impact. The PSD tiles and DIW tiles were able to enact dwell and subsequent erosion. As previously stated, future thrusts are required on the processing techniques of DIW and PSD to increase flexural strength, which could achieve the shattering mechanism during ballistic loading. The DIW tiles demonstrated less variability to ballistic penetration resistance from the 12.7-mm APM2 projectile than the PSD tiles. It was interesting to observe that, for each PSD ceramic composite, the DOP increased as yaw increased. More experiments would need to be conducted to determine if this response was a coincidence or a phenomenon.

7. References

1. King A. Ceramic technology and processing. 1st ed. Norwich (NY): William Andrew Publishing; 2002.
2. Becker B. Additive changes to advanced ceramics. Ceramic Industry; 2014 Apr 1 [accessed 2019 Mar 18]. http://www.ceramicindustry.com/articles/93848-additive-changes-to-advanced-ceramics.
3. Cesarano J III. Robocasting 3-D printing of ceramics; 2018 [accessed 2019 Mar 20]. https://www.robocasting.com.
4. ASTM C1161. Standard test method for flexural strength of advanced ceramics at ambient temperature. West Conshohocken (PA): ASTM International; 2008.
5. ASTM C1326. Standard test method for Knoop indentation hardness of advanced ceramics. West Conshohocken (PA): ASTM International; 2013.
6. Woolsey P, Kokidko D, Mariano S. Alternative test methodology for ballistic performance ranking of armor ceramics. Watertown (MA): Army Materials Technology Laboratory (US); 1989. Report No.: MTL-TR 89-43.
7. MIL-DTL-32262. Armor plate, aluminum alloy, unweldable applique 6061. Aberdeen Proving Ground (MD): Army Research Laboratory (US); 2007 July.
8. Jones T. Investigation of the kinetic energy characterization of advanced ceramics. Aberdeen Proving Ground (MD): Army Research Laboratory (US); 2015 Apr. Report No.: ARL-TR-7263.

List of Symbols, Abbreviations, and Acronyms

3-D	3-dimensional
Al_2O_3	alumina
CCDC	US Army Combat Capabilities Development Command
DIW	direct ink write
DOP	depth of penetration
EDAX	energy-dispersive X-ray spectroscopy
GT	Goodman Technologies
HEW	HotEnd Works
IP	isopressed/isopressing
PSD	pressurized spray deposition
SEM	scanning electron microscope
TD	total density

1 (PDF)	DEFENSE TECHNICAL INFORMATION CTR DTIC OCA
2 (PDF)	CCDC ARL IMAL HRA RECORDS MGMT FCDD RLD CL TECH LIB
1 (PDF)	GOVT PRINTG OFC A MALHOTRA
1 (PDF)	GOODMAN TECHNOLOGIES B GOODMAN
1 (PDF)	HOTEND WORKS LLC B BECKER
1 (PDF)	B SCOTT 65 MILLWOOD DRIVE MIDDLETOWN DE 19709
1 (PDF)	G SILSBY 303 DARLINGTON ROAD HAVRE DE GRACE MD 21078
1 (PDF)	THE NATIONAL CENTER FOR MANUFACTURING SCIENCES C BOSWELL-KOLLER
1 (PDF)	THE APPLIED RESEARCH LABORATORY THE PENNSYLVANIA STATE UNIVERSITY D SWANSON
3 (PDF)	CHIEF SCIENTIST/DIRECTOR J FOURNIER PH D LTC G WHITEHEAD C BAKER
1 (PDF)	ASSISTANT PROGRAM MANAGER SOCOM HQ FCDD SCS PS M CLARK
1 (PDF)	MATERIALS ENGINEER USSOCOM/SOF AT&L-ST C LOVELL
1 (PDF)	CCDC RDCB DEE K WALLACE
1 (PDF)	CCDC NATICK SSC M ROTH
24 (PDF)	CCDC ARL FCDD RLD H MAUPIN P PERCONTI FCDD RLD PT J WIDDER FCDD RLW T BJERKE D HOGGE FCDD RLW L T SHEPPARD FCDD RLW MD J SOUTH FCDD RLW ME J CAMPBELL J LASALVIA S SILTON L VARGAS-GONZALEZ J SWAB FCDD RLW PA S BILYK FCDD RLW PB C HOPPEL S SATAPATHY FCDD RLW PC D CASEM J CLAYTON M FERMEN-COKER C MEREDITH FCDD RLW PD J RUNYEON FCDD RLW PE T JONES P SWOBODA FCDD RLW PF N GNIAZDOWSKI FCDD RLW PG R FRANCART